Determination of Surface Recombination Velocities at Contacts in Organic Semiconductor Devices Using Injected Carrier Reservoirs

Oskar J. Sandberg,* Simon Sandén, Anton Sundqvist, Jan-Henrik Smått, and Ronald Österbacka
Center for Functional Materials and Faculty of Science and Technology, Åbo Akademi University, Porthaninkatu 3, 20500 Turku, Finland

(Received 31 August 2016; revised manuscript received 10 December 2016; published 15 February 2017)

A method to determine surface recombination velocities at collecting contacts in interface-limited organic semiconductor devices, based on the extraction of injected carrier reservoirs in a single-carrier sandwich-type structure, is presented. The analytical framework is derived and verified with drift-diffusion simulations. The method is demonstrated on solution-processed organic semiconductor devices with hole-blocking TiO_2/organic and SiO_2/organic interfaces, relevant for solar cell and transistor applications, respectively.

DOI: 10.1103/PhysRevLett.118.076601

Contacts play a crucial part in thin-film semiconductor devices, such as those based on organic and perovskite semiconductors. Most electronic devices require at least one contact that is either charge collecting or blocking. For instance, in organic field effect transistors, the source and drain constitute collecting contacts, while the gate electrode, covered with an insulating dielectric, needs to be blocking [1]. Many applications also require selective contacts that are able to efficiently either inject or collect one type of charge carrier while simultaneously blocking the other type. This is of particular importance in organic and perovskite solar cells, where contacts that are able to efficiently collect majority carriers, while simultaneously blocking minority carriers, are desired [2–9]. However, a comprehensive understanding of the processes taking place at the contacts in organic thin-film semiconductor devices is still lacking.

The current of carriers flowing out from the semiconductor (to the electrode) at a collecting contact is generally described in terms of an effective surface recombination current [10–13]:

$$J_R = qS_R[n_c - n_0], \tag{1}$$

where S_R is the associated surface recombination velocity, n_c is the carrier density at the surface and n_0 is the corresponding equilibrium density, and q is the elementary charge. The surface recombination velocity is a characteristic for the quality of the surface and can be expressed as $S_R = \sigma_R v_R N_s$, where σ_R is an *effective* capture cross section, v_R is the carrier emission velocity at the contact, and N_s is the surface density of recombination centers [3,10]. At an ideal semiconductor-metal contact, acting as an infinite recombination center ($\sigma_R N_s \to 1$), the upper limit of S_R is typically on the order of 10^6 cm/s at temperature $T = 300$ K in accordance with the thermionic emission theory [4,10]. A schematic picture of surface recombination for holes at a contact is shown in Fig. 1(a).

In general, if S_R is larger than the effective transport velocity $v_D \sim \mu|F|$ of carriers within the semiconductor layer ($S_R \gg v_D$), the carrier collection is limited by the bulk (diffusion limited) [9,14–16]. In this case, the contact virtually acts as a perfect collector ($S_R \to \infty$). Here, μ is the carrier mobility and F the electric field. If $S_R < v_D$, on the other hand, the charge collection is controlled by kinetics at the contact as the carrier transport becomes limited by the interface [9,10,16,17]. The surface recombination at a contact that is blocking from the viewpoint of carrier collection is by definition also interface limited ($S_R \ll v_D$). However, the condition $S_R \ll v_D$ alone does not necessarily fulfill the requirements of a blocking contact. Ideally, a blocking contact with $S_R = 0$ is achieved by inserting an interlayer that prevents all carriers from leaving the device at the contact ($\sigma_R N_s \to 0$). In practice, however,

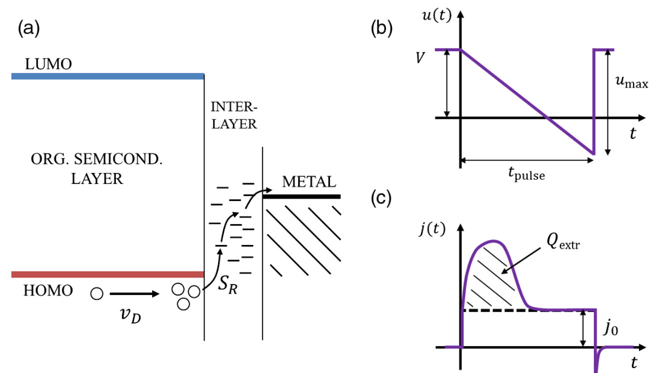

FIG. 1. (a) Schematic picture of surface recombination at a semiconductor-electrode contact for holes being collected at a metal electrode. In (b) and (c), a schematic picture of the CELIV technique is shown. A linear voltage pulse $u(t)$ is applied to extract charge carriers at the dc voltage V. From the corresponding extraction current transient $j(t)$ (corrected for the steady-state current), the extracted charge is obtained from $Q_{extr} = \int_0^{t_{extr}}[j(t) - j_0]dt$, where $j_0 = (\varepsilon\varepsilon_0/d)(du/dt) = (\varepsilon\varepsilon_0 u_{max}/dt_{pulse})$.

 © 2017 American Physical Society

recombination centers (gap states) are likely to always be present within the interface layer ($\sigma_R N_s \neq 0$) [2,3,10,13,18], effectively leading to nonzero S_R [see Fig. 1(a)]. The surface recombination velocity is thus a key parameter in understanding the processes taking place at the contacts.

In this Letter, a method to determine the surface recombination velocity at limiting contacts in organic semiconductor devices is proposed. The method is based on the analytical derivation of the relationship between the net charge, injected into the semiconductor layer in a single-carrier device structure, and the surface recombination velocity at the collecting contact. By determining the injected charge by charge extraction measurements, the surface recombination velocity is subsequently obtained. The method can be used to investigate properties of (nominally) blocking buffer layers, such as selective electrode interlayers and gate dielectrics, in organic semiconductor devices.

The device under consideration is hole-only consisting of a semiconductor layer, sandwiched between a hole-injecting contact at the anode ($x = 0$) and a hole-collecting contact with a finite S_R for holes at the cathode ($x = d$), where d is the thickness of the semiconductor layer. By applying a dc voltage $V > V_{\mathrm{bi}}$, where V_{bi} is the (effective) built-in voltage of the device, holes are readily injected into the semiconductor layer from the injecting anode contact. The net injected charge accumulating in the layer is given by $\Delta Q = q\int_0^d \Delta p(x)dx$, where $\Delta p(x) = p(x) - p_0(x)$ is the difference between the hole density at the applied voltage V and the equilibrium hole density. The surface recombination current at the collecting cathode contact is given by $J_p|_{\mathrm{cat}} = qS_R\Delta p(d)$, where $p(d)$ is the hole density at the cathode interface. The impact of S_R for holes at the cathode is simulated in Fig. 2. For the simulations, a previously developed drift-diffusion-Poisson model is used [17]. Typical energy level diagrams for the case $S_R < v_D$ are shown in Fig. 2(a). In Fig. 2(b), the simulated ΔQ as a function of V at different surface recombination velocities is shown, as depicted by the symbols. At high S_R, in this case larger than 0.10 cm/s, ΔQ is independent of S_R. This corresponds to the bulk-limited regime $S_R \gg v_D$, when ΔQ is independent of the kinetics at the cathode interface. Note that, close to flat-band conditions ($V = V_{\mathrm{bi}}$), $v_D \approx \mu kT/qd$ corresponding to 0.13 cm/s in this case. At smaller S_R, however, a drastic increase in ΔQ with decreasing S_R and increasing V is obtained.

The behavior in the $S_R \ll v_D$ limit can be understood as follows. For a planar hole-only device, the steady-state continuity equation requires that $dJ_D/dx = 0$, where J_D is the current density. Hence, the size of the accumulated reservoir of bias-induced holes is controlled by the current density flowing through the device $J_D(V) = J_p|_{\mathrm{cat}} = qS_R\Delta p(d)$, being dependent on both S_R and V. As more holes are being transported to the cathode interface than holes leaving the device at the cathode, the injected holes will accumulate at the cathode interface. Under these circumstances ($S_R \ll v_D$), the quasi-Fermi-level E_{Fp} is flat in the active layer at quasiequilibrium conditions [9,10,16]. The hole density is given by $p(x) = N\exp([E_v(x) - E_{Fp}]/kT) = p(d)\exp([E_v(x) - E_v(d)]/kT)$, where N is the density of transport states, k is the Boltzmann constant, and $E_v(x)$ is the (effective) hole transport level. Upon solving the Poisson equation,

$$\frac{1}{q}\frac{d^2E_v(x)}{dx^2} = \frac{qp(x)}{\varepsilon\varepsilon_0}, \tag{2}$$

where $\varepsilon\varepsilon_0$ is the permittivity, the injected hole density near the cathode interface can be expressed as $p(x) = p(d)/(1 + [d - x]/\lambda\sqrt{2})^2$, with the Debye length $\lambda = \sqrt{\varepsilon\varepsilon_0 kT/q^2 p(d)}$ [10,19,20]. In the derivation of $p(x)$, it was assumed that a minimum for $E_v(x)$ exists within the active layer at a distance $\gg\lambda$ from the cathode interface. The injected charge, accumulating at the cathode interface, becomes

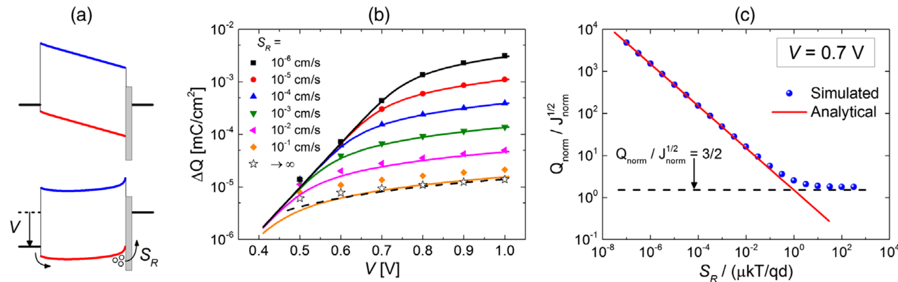

FIG. 2. (a) Simulated energy level diagrams at $V = 0$ (upper) and $V > V_{\mathrm{bi}}$ (lower) are shown for the case $S_R < v_D$ at the cathode ($x = d$). In (b), the simulated ΔQ as a function of applied voltage V for varying S_R is indicated by symbols. The analytical approximation Eq. (3) is depicted by the corresponding solid lines. The current density $J_D(V)$ is obtained from the simulated JV curve (not shown). The dashed line corresponds to $\Delta Q = \frac{3}{2}CU$. In (c), the normalized $Q_{\mathrm{norm}}/J_{\mathrm{norm}}^{1/2}$ as a function of $S_R/(\mu kT/qd)$ is shown, where $Q_{\mathrm{norm}} \equiv \Delta Q/CU$, $J_{\mathrm{norm}} \equiv J_D/J_{\mathrm{SCLC}}$, and $\mu kT/qd \approx 0.13$ cm/s. In the simulations we assume $V_{\mathrm{bi}} = 0.5$ V, $d = 200$ nm, $\varepsilon = 3$, $T = 300$ K, $\mu = 10^{-4}$ cm^2/V s, and an injection barrier of 0.20 eV at the anode.

$$\Delta Q \approx \sqrt{2\epsilon\epsilon_0 kT p(d)} = \sqrt{\frac{2\epsilon\epsilon_0 kT}{qS_R} J_D(V)}, \qquad (3)$$

for $p(d) = J_D(V)/qS_R \gg p_0(d)$. Indeed, upon comparing Eq. (3) (solid lines) with the simulated ΔQ (symbols) in Fig. 2(b), an excellent agreement is found for $V > V_{\rm bi}$.

In Fig. 2(c), the ratio $\Delta Q/J_D^{1/2}$ is simulated as a function of $S_R/(\mu kT/qd)$. Note that Eq. (3) can be reexpressed as $\Delta Q\sqrt{(J_{\rm SCLC}/J_D)} = 1.5CU\sqrt{(\mu kT/qS_R d)}$, where $C = \epsilon\epsilon_0/d$ is the geometric capacitance of the semiconductor, $J_{\rm SCLC} = 9\epsilon\epsilon_0\mu U^2/8d^3$ is the space-charge-limited current density (see Refs. [15,21]), and U is the (effective) potential difference across the layer. Comparing the analytical prediction with the simulations, we see that an excellent agreement is obtained when $S_R < \mu kT/qd$. On the other hand, as $S_R > \mu kT/qd$, the charge transport is no longer limited by the kinetics at the cathode. In this case, the injected charge instead approaches $\Delta Q = \frac{3}{2}CU$ as $J_D \to J_{\rm SCLC}$, as expected from the theory of bulk-limited charge transport [21].

Experimentally, the injected charge at V can be quantified by applying a voltage pulse $u(t)$ of reversed polarity (relative to V) and measuring the induced extraction current transient $j(t)$. In this work, we use charge extraction by a linearly increasing voltage (CELIV) pulse to extract the injected charge [22–24]; a schematic picture is shown in Figs. 1(b) and 1(c). For a hole-only device, the extracted charge can generally be expressed as [25]

$$Q_{\rm extr} \equiv \int_0^{t_{\rm extr}} [j(t) - j_0 - J_D]dt = -\frac{q}{d}\int_0^d \int_x^d \Delta p dx' dx, \qquad (4)$$

where $j_0 = C(du/dt)$ and $t_{\rm extr}$ is the time at which the injected bias-induced carriers have been extracted. In our case of an injected surface charge of holes at the cathode, we find $|Q_{\rm extr}| \approx \Delta Q$, provided that $\lambda \ll d$. As a result, the extracted charge at $V > V_{\rm bi}$ can be used to determine the surface recombination velocity at the contact via

$$S_R = \frac{2\epsilon\epsilon_0 kT}{qQ_{\rm extr}^2} J_D(V), \qquad (5)$$

where $J_D(V)$ is the steady-state current density at $V > V_{\rm bi}$, obtained from the dark current-voltage characteristics. The determination of S_R is limited to the case $S_R < v_D$. If $S_R \gg v_D$, however, Eq. (5) instead gives an effective (bulk-limited) transport velocity $S_R^{\rm eff} \approx \mu kT/qd$ at the contact, corresponding to a lower limit estimate of S_R. In the following, the method is demonstrated on solution-processed organic semiconductor devices, employing TiO_2 and SiO_2 as electrode buffer layers (for experimental details, see Supplemental Material [26]).

We first demonstrate the method on an inverted organic solar cell device with TiO_2 as the cathode interlayer. TiO_2 has been commonly used as an electron-selective (hole-blocking) layer in organic, dye-sensitized, and perovskite solar cells [2,7,30]. The organic semiconductor layer consists of P3HT:PCBM, widely studied in organic solar cell research. The hole-only device structure is ITO/TiO_2(7 nm)/P3HT:PCBM/Cu, where Cu is used as the hole-injecting anode. By applying a positive dc bias, holes are accumulated at the TiO_2/P3HT:PCBM interface. These charges are subsequently extracted using CELIV. In Figs. 3(a) and 3(b), the extracted charge and steady-state current density are shown at different dc voltages V, respectively. The corresponding surface recombination velocities S_R (symbols), as calculated using Eq. (5), are presented in Fig. 3(c). The analysis yields a surface recombination velocity of $S_R \approx 6 \times 10^{-6}$ cm/s for holes at the TiO_2/P3HT:PCBM interface, consistent with findings in Ref. [24]. This is to be compared to $v_D \sim \mu kT/qd$ estimated to be 0.06 cm/s. Introducing the hole-blocking TiO_2 layer effectively reduces the hole transport velocity by a factor of 10^4 at the cathode contact. However, a small number of holes are still able to leak through the TiO_2 layer, suggesting that recombination (with electrons in the cathode layer) is taking place at the TiO_2/organic contact (cf. Fig. 1).

In general, there are also parasitic conductive pathways present for the current to circumvent the device (or the blocking layer), giving rise to additional leakage currents.

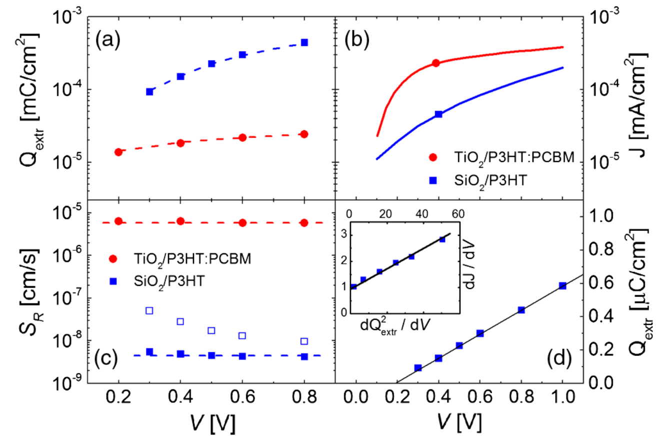

FIG. 3. In (a) and (b), the extracted charge $Q_{\rm extr}$ and steady-state current density J, respectively, are shown for TiO_2/P3HT:PCBM (circles) and SiO_2/P3HT (squares) interfaces at different V. In (c), the corresponding S_R for holes is shown, as obtained by Eq. (5) (symbols). The open and solid squares indicate SiO_2/P3HT data that have been uncorrected ($R_{\rm sh} = \infty$) and corrected ($R_{\rm sh} \approx 1050\ \Omega\,{\rm m}^2$) for the shunt resistance, respectively. The dashed lines in (a) and (c) correspond to $S_R = 5.8 \times 10^{-6}$ cm/s and $S_R = 4.5 \times 10^{-9}$ cm/s for TiO_2/P3HT:PCBM and SiO_2/P3HT, respectively. In (d), the extracted charge for SiO_2/P3HT [from (a)] is shown on the linear scale (symbols); the corresponding dJ/dV [mS/m^2] as a function of $dQ_{\rm extr}^2/dV$ [(C/m^2)^2/MV] are shown in the inset.

These leakage currents are typically described in terms of a finite shunt resistance. Taking this effect into account, the total measured current density is given by

$$J(V) = J_D(V) + V/R_{\mathrm{sh}}, \tag{6}$$

where R_{sh} is the effective shunt resistance in units of $\Omega \cdot \mathbf{m}^2$. Neglecting the presence of a finite shunt resistance leads to an overestimation of $J_D(V)$ and thereby also S_R. Based on Eq. (6), the effect of shunts can be taken into account by differentiating with respect to V and making use of Eq. (5); one finds

$$\frac{dJ(V)}{dV} = \frac{1}{R_{\mathrm{sh}}} + \frac{qS_R}{2\varepsilon\varepsilon_0 kT}\frac{d[Q_{\mathrm{extr}}^2]}{dV}, \tag{7}$$

assuming S_R to be independent of V. By plotting $dJ(V)/dV$ as a function of dQ_{extr}^2/dV, the shunt resistance is obtained from the intercept, while S_R is obtained from the slope. For the TiO_2/P3HT:PCBM device, the effect of shunts was found to be insignificant.

In Fig. 3, we also included an organic semiconductor device of P3HT with a thin insulating SiO_2 layer, typically used as a gate dielectric in transistor applications [1], at the cathode. The device structure is given by ITO/SiO_2(5 nm)/P3HT/MoO_3/Ag with MoO_3/Ag as the hole-injecting anode. The accumulated charge at the SiO_2/P3HT interface is found to be closely given by $Q_{\mathrm{extr}} = C_i U$ [see Fig. 3(d)], where C_i is the geometric capacitance of the SiO_2 layer. Because of the low current densities obtained in this case, shunts will dominate at smaller voltages. Utilizing Eq. (7), we obtain $R_{\mathrm{sh}} \approx 1050\ \Omega \cdot \mathbf{m}^2$. The effect of shunts on the extracted S_R is demonstrated in Fig. 3(c). After correcting the current for the shunt, we find $S_R \approx 5 \times 10^{-9}$ cm/s for holes at the SiO_2/P3HT interface. It should be noted that if shunts are not accounted for, Eq. (5) instead gives an upper limit estimate of S_R.

The above analysis based on Eq. (3) assumes the nondegenerate limit to be valid. At very high carrier concentrations (low S_R and high V), however, density of states (DOS) filling effects become significant [28]. Under these conditions, the shape of the DOS can be taken into account via a correction factor η, and we obtain $S_R = \eta S_R^0$ (see Supplemental Material [26]), where S_R^0 corresponds to the nondegenerate case given by Eq. (5). In the case of a Gaussian distribution of states [$\propto \exp(-E^2/2\sigma^2)$], η is well approximated by $\eta \approx 1/\mathrm{erf}([-\ln c]^{2/3} kT/\sigma)$ for $c \leq 0.1$, where $c = p(d)/N$ is the DOS occupation and σ is the energetic disorder parameter (see Supplemental Material [26]). Concomitantly, with $\sigma = 69$ meV for P3HT [29], η is close to 1.5 for $c = 0.1$ (at 300 K). At smaller c, the nondegenerate limit is eventually approached as $\eta \to 1$.

In conclusion, a technique to determine (effective) surface recombination velocities at contacts in thin-film devices is presented. The method is based on using a single-carrier device structure with an injecting contact to inject and accumulate a carrier reservoir at the opposite collecting contact interface. From the size of the injected charge reservoir, determined by charge extraction measurements, the surface recombination velocity for carriers accumulating at the collecting contact can be obtained. The analytical framework behind the method is derived and confirmed by numerical simulations. Furthermore, the method is demonstrated on hole-only organic thin-film devices with different hole-blocking buffer layers.

Helpful discussions with Professor Gytis Juska and Dr. Kristijonas Genevicius are greatly acknowledged. The Academy of Finland is acknowledged for funding through Projects No. 279055 and No. 259310. O. J. S. acknowledges funding from the Magnus Ehrnrooth Foundation.

*osandber@abo.fi

[1] H. Sirringhaus, Adv. Mater. **26**, 1319 (2014).
[2] E. L. Ratcliff, B. Zacher, and N. R. Armstrong, J. Phys. Chem. Lett. **2**, 1337 (2011).
[3] P. Würfel, *Physics of Solar Cells, Physics of Solar Cells*, 2nd ed. (Wiley-VCH, Weinheim, 2009).
[4] T. Kirchartz, B. E. Pieters, K. Taretto, and U. Rau, Phys. Rev. B **80**, 035334 (2009).
[5] W. Tress, K. Leo, and M. Riede, Phys. Rev. B **85**, 155201 (2012).
[6] E. L. Ratcliff, A. Garcia, S. A. Paniagua, S. R. Cowan, A. J. Giordano, D. S. Ginley, S. R. Marder, J. J. Berry, and D. C. Olson, Adv. Energy Mater. **3**, 647 (2013).
[7] E. J. Juarez-Perez, M. Wussler, F. Fabregat-Santiago, K. Lakus-Wollny, E. Mankel, T. Mayer, W. Jaegermann, and I. Mora-Sero, J. Phys. Chem. Lett. **5**, 680 (2014).
[8] J. Reinhardt, M. Grein, C. Bühler, M. Schubert, and U. Würfel, Adv. Energy Mater. **4**, 1400081 (2014).
[9] O. J. Sandberg, A. Sundqvist, M. Nyman, and R. Österbacka, Phys. Rev. Applied **5**, 044005 (2016).
[10] S. M. Sze, *Physics of Semiconductor Devices* (Wiley, New York, 1981).
[11] P. S. Davids, I. H. Campbell, and D. L. Smith, J. Appl. Phys. **82**, 6319 (1997).
[12] J. C. Scott and G. C. Malliaras, Chem. Phys. Lett. **299**, 115 (1999).
[13] A. Wagenpfahl, D. Rauh, M. Binder, C. Deibel, and V. Dyakonov, Phys. Rev. B **82**, 115306 (2010).
[14] J. G. Simmons, Phys. Rev. Lett. **15**, 967 (1965).
[15] P. de Bruyn, A. H. P. van Rest, G. A. H. Wetzelaer, D. M. de Leeuw, and P. W. M. Blom, Phys. Rev. Lett. **111**, 186801 (2013).
[16] C. R. Crowell and S. M. Sze, Solid State Electron. **9**, 1035 (1966).
[17] O. J. Sandberg, M. Nyman, and R. Österbacka, Phys. Rev. Applied **1**, 024003 (2014).
[18] S. Wheeler, F. Deledalle, N. Tokmoldin, T. Kirchartz, J. Nelson, and J. R. Durrant, Phys. Rev. Applied **4**, 024020 (2015).
[19] Yu. A. Genenko, S. V. Yampolskii, C. Melzer, K. Stegmaier, and H. von Seggern, Phys. Rev. B **81**, 125310 (2010).

[20] P. Nelson, *Biological Physics: Energy, Information, Life* (W. H. Freeman, New York, 2004).

[21] M. A. Lampert and P. Mark, *Current Injection in Solids* (Academic, New York, 1970).

[22] G. Juska, N. Nekrasas, and K. Genevicius, J. Non-Cryst. Solids **358**, 748 (2012).

[23] S. Sandén, O. Sandberg, Q. Xu, J.-H. Smått, G. Juska, M. Lindén, and R. Österbacka, Phys. Chem. Chem. Phys. **14**, 14186 (2012).

[24] A. Sundqvist, O. J. Sandberg, M. Nyman, J-H. Smått, and R. Österbacka, Adv. Energy Mater. **6**, 1502265 (2016).

[25] S. A. Hawks, B. Y. Finck, and B. J. Schwartz, Phys. Rev. Applied **3**, 044014 (2015).

[26] See Supplemental Material at http://link.aps.org/supplemental/10.1103/PhysRevLett.118.076601 for experimental details, additional derivations and simulations, which includes Refs. [27–29].

[27] S. Sandén, O. Sandberg, Q. Xu, J.-H. Smått, G. Juska, M. Lindén, and R. Österbacka, Org. Electron. **15**, 3506 (2014).

[28] G. Paasch and S. Scheinert, J. Appl. Phys. **101**, 024514 (2007).

[29] J. Lorrmann, M. Ruf, D. Vocke, V. Dyakonov, and C. Deibel, J. Appl. Phys. **115**, 183702 (2014).

[30] M. Grätzel, Acc. Chem. Res. **42**, 1788 (2009).